Emergent Tissue Shapes from the Regulatory Feedback between Morphogens and Cell Growth

Bivash Kaity[1] and Daniel Lobo[1,2,*]

[1] Department of Biological Sciences
University of Maryland, Baltimore County
1000 Hilltop Circle
Baltimore, MD 21250, USA.

[2] Center for Stem Cell Biology & Regenerative Medicine and
Marlene and Stewart Greenebaum Comprehensive Cancer Center
University of Maryland, School of Medicine
22 S. Greene Street
Baltimore, MD 21201, USA.

[*] Corresponding author
E-mail: lobo@umbc.edu
Tel: (410) 455-5726

Short title: The feedback between morphogens and shape

Abstract

Patterning and morphogenesis in multicellular organisms require precise dynamic coordination between cellular behaviors and mechano-chemical signals. However, the mechanisms underlying the pathways that coordinate and integrate these signals into emergent cellular behaviors and tissue shapes remain poorly understood. Here, we present a cell-centered agent-based mathematical approach to shed light on the feedback mechanisms underlying tissue growth and pattern formation. The model includes cell size dynamics governed by both intercellular diffusible morphogen concentrations and mechanical stress between cells to control their spatial organization, and does not require the use of any superimposed lattice, increasing its applicability and performance. The results show how the precise integration of the feedback loop between cellular behaviors and mechano-chemical signaling is essential for the regulation of shape and spatial patterns across the tissue scale. Furthermore, the regulation of cellular dynamics by patterning processes, such as Turing activator-inhibitor systems, can drive the formation of emergent stable tissue shapes, which, in turn, specify the domain for morphogen patterning—closing the self-regulated loop between tissue shape and morphogenetic signals. Overall, this study highlights the importance of the feedback loop between morphogen patterning and cellular behaviors in regulating tissue growth dynamics and stable shape formation. Moreover, this study establishes a framework for further experiments to understand the regulatory dynamics of whole-body development and regeneration using high spatiotemporal resolution models.

Significance

Tight coordination and interpretation of the multitude of signals at different biological scales are essential during the development of multicellular organisms to control their shape, size, and pattern. In this work, we investigated the leading role of the feedback between mechano-chemical signaling networks and tissue shape through cellular behaviors such as growth, proliferation, and apoptosis. The model explains the interdependence between tissue growth and pattern formation mechanisms in regulating the fundamental properties of morphogenesis. Overall, this study provides mechanistic insights into the regulatory feedback interactions between tissue morphogenesis and patterning dynamics.

Keywords: Morphogenesis and patterning; Tissue growth dynamics; Emergent tissue shapes, Mechanochemical feedback; Multiscale modeling; Morphogenetic feedback loop; Computational morphogenesis; Agent-based modeling.

1. Introduction

Patterning, cell growth, and differentiation are complex interconnected processes that drive the development of multicellular organisms. Crucially, they act at different scales to modulate cellular mechanisms (1), such as migration, proliferation, apoptosis, and division orientation (2). In addition, biochemical signaling is essential for establishing the graded distribution of morphogens, leading to the emergence of shapes and forms (3–5). While it is known that the coordination and dynamic synchronization of cellular behaviors regulate an organism's size, shape, and function (6–8), the mechanistic understanding of the feedback regulation between signaling and tissue growth during development and regeneration remains unclear.

The complex feedback loops between chemical signaling and mechanical cellular interactions regulate patterns and growth, and hence the emergence of shapes and forms. Dysregulation of this network may lead to abnormalities in tissue shape and function (12, 13). Several mechanisms have been studied to explain the emergence of tissue shapes from mechanical interactions, including cell-cell adhesion through extracellular matrix components (14–16). In addition, repulsive forces due to the elastic properties of cells inhibit the deformation of cell morphology, which can also guide tissue patterning (17). Indeed, the interaction range between cells is a crucial factor for their spatial organization and the resulting tissue shape, including long distance cell-cell interactions essential for spreading epithelial cells (18). In addition to mechanical interactions, chemical signals acting as morphogens significantly contribute to the regulation of cell growth, proliferation, and death, which are necessary for proper tissue morphogenesis (19). For example, sonic hedgehog (*Shh*) is an essential driver of tissue morphogenesis, regulating properties such as patterning, proliferation, growth, and differentiation (20). *Shh* interacts with other gene regulators to form activator-inhibitor networks that control the development of many body structures, such as feather patterning (21), ruggae in the mammalian palate (22), and scutes in turtle shells (23). Therefore, the feedback between biochemical and mechanical signals plays a fundamental role in driving tissue morphogenesis by regulating cellular behavior (24, 25). However, owing to the complexity of these feedback loops and their emergent behaviors, understanding how cell mechanisms are regulated to produce precise and robust shapes and patterns at the tissue scale remains a challenge.

To understand the feedback between cell behaviors, signaling, and emergent tissue growth, mathematical and computational approaches are fundamental for modeling cell-level phenomena

and explaining the resulting tissue-level forms to understand the feedback between cell behaviors, signaling, and emergent tissue growth (26, 27). Among them, approaches based on off-lattice, cell-center models can simulate discrete cells with free tissue growth dynamics without limited spatial resolution, in contrast to continuous or agent-based approaches based on a fixed lattice (28–31). In this way, cell positions in these models are continuous in space, and the emergent high-resolution tissue behaviors result from intercellular mechanical forces (32). However, integrating regulatory signaling pathways, including intercellular communication within growing tissues, is challenging because of the dynamics of cell proliferation and death, as well as the resulting tissue density and boundaries (33, 34). Off-lattice models can couple cellular and chemical submodels by simulating reaction-diffusion systems in superimposed meshes derived from cellular positions (35–38). However, extracellular tissue meshes are the most critical components of this modeling approach, as high-resolution spatial meshes are necessary to accurately simulate tissue growth dynamics. High-resolution meshes substantially increase the computational costs, especially when cells proliferate, die, or migrate. As a result of each of these processes, a recomputed tissue mesh is necessary, further increasing the computational costs and reducing the efficiency. The lattice structure can also introduce a significant challenge in developing dynamic feedback networks between cell- and tissue-level phenomena by coupling all regulatory inputs to reveal tissue morphogenetic and patterning processes. Thus, these challenges limit the scalability and applicability of lattice-based extracellular environment models for large-scale or long-term simulations and have led to increased interest in off-lattice modeling approaches for studying tissue growth.

Here, we propose a lightweight mathematical and computational model of coupled cellular mechanics, signaling, and growth to study how their feedback loops can control tissue patterning and shape. The model is based on a lattice-free, agent-based framework that combines the roles of biochemical and mechanical signals at the cellular level to study the emergent properties at the tissue level. The mechanical submodel quantifies the physical and adhesive properties of cells and describes their coordinated movements and arrangements (7, 9, 39). The chemical signaling submodel describes the dynamics of both diffusive morphogens at the tissue level and the intracellular gene regulatory network at the cellular level (6, 22). Crucially, cells define both the intercellular space for gene regulatory mechanisms and the tissue space where intracellular signals diffuse, reducing the complexity and computational requirements of the model. We hypothesized

that cell size dynamics are influenced by two factors: the level of growth morphogen and the amount of mechanical stress caused by cell density. The results show how the dynamics of growth morphogens play a critical role in regulating the shape and size of emergent tissues. We then extended the model with a Turing activator-inhibitor regulatory mechanism controlling cell growth dynamics, which can lead to different stable tissue shapes through the feedback mechanism between the tissue pattern and shape. Overall, the proposed framework provides a comprehensive understanding of morphogenesis through the feedback regulation between intracellular signals and the emergent tissue shapes through cell-level phenomena, such as motility, growth, division, degrowth, and death.

2. Methods

2.1. Cells

We define a two-dimensional model of a tissue or whole organism made of a dynamic collection of cells, each considered a circular disc capable of migration, growth, division, and apoptosis. The disc center x_i represents the position of cell i, and the disk radius r_i defines its size. Therefore, a system of N cells at a given time is defined as a set of points $\{x_1, x_2, \dots, x_N\}$ and associated radii $\{r_1, r_2, \dots, r_N\}$, with $x_i \in R^2$ and $r_i \in R$. The movement of each cell i in the system is governed by Newton's law of motion, such as

$$m_i \ddot{x}_\iota = F_i, \tag{1}$$

where m_i is the cell mass and F_i represents the sum of all forces acting on the cell.

Each cell i is subjected to a viscous force F_i^{vis} and an interaction force F_i^{int}, such that

$$F_i = F_i^{vis} + F_i^{int}. \tag{2}$$

The viscous force occurs in the opposite direction of motion and is due to the interaction of a cell with the extracellular matrix and media, such that

$$F_i^{vis} = -\xi \dot{x}_\iota, \tag{3}$$

where ξ is the viscous coefficient. Since the acceleration due to the inertial force is negligible compared to the effect of the viscous force in the cell microenvironment (40–42), the equation of motion becomes

$$\xi \dot{x}_i = F_i^{int}. \tag{4}$$

We assume the interaction force F_i^{int} to be the sum of all pairwise interaction forces between cells and hence

$$F_i^{int} = \sum_{i=1, j \neq i}^{N} F_{ij}\,, \tag{5}$$

where F_{ij} is the interaction force between cell i and j. The pairwise interaction force is rotationally invariant and comprises attractive and repulsive components. An attractive component represents the adhesion between two cells, whereas the repulsive component opposes the deformation of cells owing to their elastic properties. Hence, we model the cell-cell interaction as a linear spring force together with a quadratic term that approximates the contact area between two cells (39) such that

$$F_{ij} = \begin{cases} \mu\left(d_{ij} - d_{max}\right)^2 \left(d_{eq} - d_{ij}\right) u_{ij} & \text{if } d_{ij} \leq d_{max}, \\ 0 & \text{otherwise,} \end{cases} \tag{6}$$

where μ is the cell interaction strength constant, d_{ij} is the distance between the two interacting cells defined as $d_{ij} = \|x_i - x_j\|$, d_{eq} is the equilibrium distance defined as the sum of the radii of the two cells such that $d_{eq} = r_i + r_j$, d_{max} is the maximum interacting distance between cells, and u_{ij} is the unit vector defining the force direction as $u_{ij} = \frac{x_j - x_i}{d_{ij}}$.

2.2. Morphogens

Cells can express morphogens that diffuse into neighboring cells. The system of N cells can express K different morphogens, such as each cell i contains a homogeneous concentration m_{ik} for each morphogen k, with $m_{ik} \in R$. The concentration dynamics of each morphogen is defined as

$$\dot{m}_{ik} = R_{ik} + D_{ik}, \tag{7}$$

where R_{ik} is the reaction term and D_{ik} is the diffusion term of morphogen k in cell i. Intracellularly, morphogen k concentration in cell i changes due to production, degradation, and dilution, such as

$$R_{ik} = Q_{ik} - \lambda_k m_{ik} - g_i m_{ik}, \tag{8}$$

where Q_{ik} is the production term that depends on the particular regulation modeled, λ_k is the decay constant, and g_i is the growth rate of the cell. Morphogen diffusion occurs across neighboring cells and is approximated as a rate equation (43), such as

$$D_{ik} = \frac{\alpha_k}{\pi r_i^2} \sum_{\substack{j \neq i \\ d_{ij} < d_{max}}} \frac{d_{max} - d_{ij}}{d_{max} - d_{eq}} (m_{jk} - m_{ik}), \tag{9}$$

where α_k is the diffusion constant and πr_i^2 represents the cell area. In this way, the effective diffusion coefficient becomes α_k when two cells are at equilibrium distance d_{eq} of each other, but 0 when they are at or beyond their maximum interaction distance d_{max}.

2.3. Cell size dynamics

A growth morphogen with concentrations m_{i1} for each cell i regulates cell size dynamics. Depending on the local concentration of the growth morphogen, cells can grow or degrow exponentially, which in turn can trigger their mitosis or apoptosis when their size is doubled or halved, respectively. Mitosis replaces the parent cell centered at x_i with two overlapping daughter cells, each half the parent size and centered at $x_i \pm \left(1 - \sqrt{\frac{1}{2}}\right) r_i u_U$, where u_U is a unit vector with a uniform random direction, such that the daughter cells are maximally separated but within the area of the parent cell (Figure 1). Apoptosis removes the cell from the system. In addition, cell growth is modulated by the local cell density, which can inhibit cell growth due to crowding. Thus, the growth rate g_i for cell i is defined as

$$g_i = \left((g_{max} - g_{min}) \frac{{m_{i1}}^h}{k^h + {m_{i1}}^h} + g_{min} \right) \left(\frac{c^h}{c^h + n_i^h} \right), \tag{10}$$

where g_{max} and g_{min} are the maximum and minimum cell growth rate constants, respectively, m_{i1} is the growth morphogen concentration in cell i, k is the half-maximum concentration of the growth morphogen, h is the Hill coefficient, n_i is the number of neighbors of cell i within distance d_{max}, and c is the half-maximum crowding inhibition. Then, the cell growth rate g_i modulates the area A_i of cell i as

$$\dot{A}_i = g_i A_i. \tag{11}$$

For all simulations, we set $g_{max} = 0.01$ and $g_{min} = -0.01$ so that the half-maximum concentration k denotes the growth morphogen concentration at which the growth rate is zero. When the growth morphogen concentration is higher or lower than k, cells grow towards mitosis or shrink towards apoptosis, respectively. In addition, we set h=8.

2.4. Numerical methods

The system of equations was implemented and solved with MATLAB (MathWorks, Inc.) using the standard Euler forward scheme with a sufficiently small time-step of $\Delta t = 0.001$. To optimize computational time, projection sorting (44) was implemented for determining cell neighbors.

3. Results

3.1. Whole-body modeling framework

To study the feedback regulation between morphogens and shape in multicellular tissues and whole organisms, we present a modeling framework comprising off-lattice, agent-based cells that can migrate, grow, divide, and die as they are regulated by diffusive morphogens expressed by the cells (Figure 1). Cells interact with each other through attractive forces due to adhesion and repulsive forces due to deformation, which can produce stable tissue shape configurations. Crucially, morphogens can control cell growth rates and diffuse across cells but not externally outside the tissue, which allows the modeling of self-contained systems, such as an organ or whole organism. In this way, the cells in the system can form one or more independent tissues, each made of a set of interconnected cells where the morphogens can be expressed and diffuse within but not across the tissue boundary. In response to these morphogen concentrations, cells can grow or shrink, resulting in mitosis when the cell size is doubled or apoptosis when it is halved (45). The

feedback loop between the biochemical signals forming spatial patterns and the mechanical forces between cells gives rise to the overall emergent shape of the whole tissue or organism.

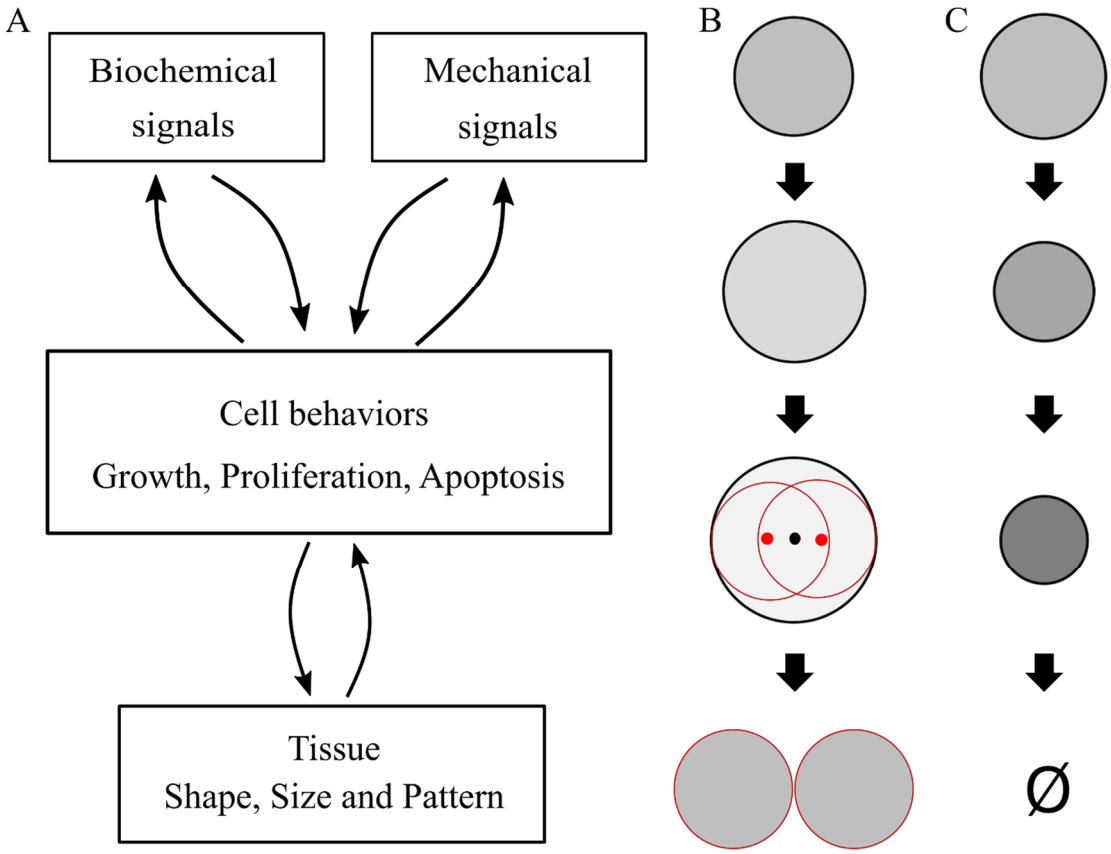

Figure 1. Proposed modeling framework for the regulation of whole-body shape dynamics. A. The model includes multiple layers of regulation that form feedback loops and give rise to emergent morphogen patterning and tissue morphogenesis. **B.** Cell area duplication results in mitosis. **C.** Cell area halving results in apoptosis.

3.2. Regulation of shape and size by a single morphogen-source cell

We sought to test the proposed model with a simulation of shape regulation from a single point source and investigate how tissue size and shape are modulated by the different biological parameters. The initial state includes two cells: a source cell expressing the diffusible growth morphogen at a constant rate q and a target cell (and its progeny) responding to the same morphogen. Hence, the production term Q_{i1} for each cell i is defined as

$$Q_{i1} = \begin{cases} q & \text{if } i = 1, \\ 0 & \text{otherwise.} \end{cases} \tag{12}$$

The morphogen expressed from the single source diffuses to neighboring cells and degrades at a constant rate (Equation 8). The source cell has a constant volume and does not divide or die. The target cell and its progeny can divide or die through apoptosis in response to their size, which is regulated by the growth morphogen (Equation 10).

Figure 2A shows the tissue growth dynamic simulation as regulated by a single source cell (see Supplementary Video 1). The growth morphogen is expressed by the source cell (red) and diffuses through the cell population, creating a radial morphogen gradient. This gradient modulates the proliferative behavior of the cells, resulting in tissue growth in all directions, which then surrounds the source cell at the center. The system reaches a steady state, forming a circular shape, in which the growth morphogen has a maximum concentration at the center, in the source cell, and a minimal concentration at the tissue shape edge. This concentration gradient produces a differential growth rate in the population, where cells near the center grow and divide and those away from the center degrow and then die. At the steady state, the frequency of mitosis and apoptosis events balance out and the number of cells in the tissue becomes constant. Thus, a single source cell causes the population to converge to a steady state with a circular shape.

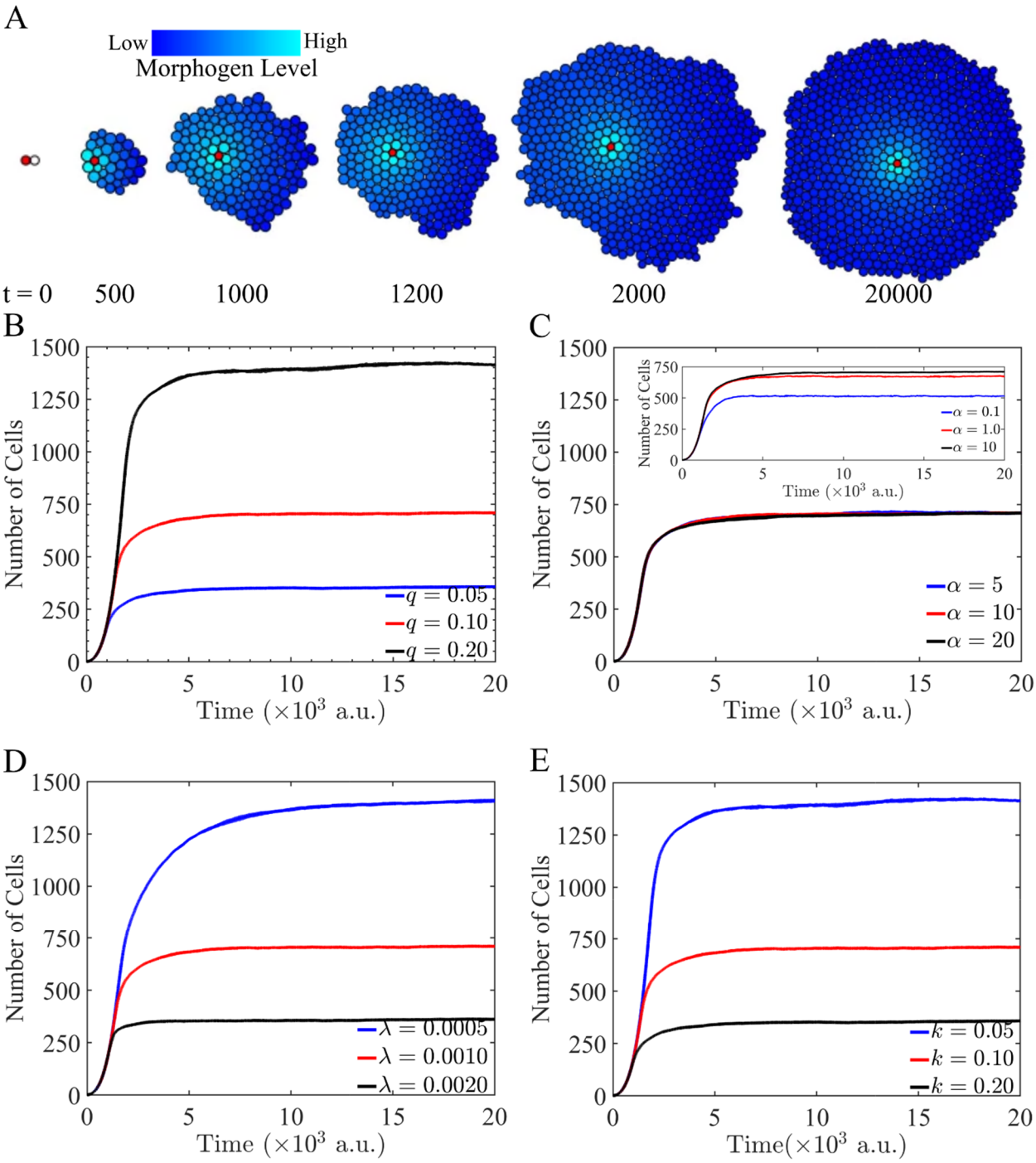

Figure **2. A single source cell secreting a growth morphogen produces a steady-state circular shape that is modulated by the morphogen properties. A.** Tissue growth controlled by a diffusing growth morphogen (blue) expressed from a single source cell (red) results in a steady-state circular shape. Parameters as red lines in panels B-E. **B.** The total number of cells at steady state linearly depends on the morphogen production constant (q). **C.** The morphogen diffusion constant (α) has a weaker effect on the

total number of cells at the steady state. **D.** The morphogen degradation rate (λ) has an inverse effect compared to the production rate, albeit at a slower rate. **E.** The morphogen regulation threshold (k) between growth and degrowth has a similar but inverse effect compared to the morphogen production rate. All parameter sets were simulated ten times. The plots show the average (line) and standard deviation (shaded area). Except where indicated, the parameters were $q = 0.1$, $\alpha = 10$, $\lambda = 0.001$, $k = 0.1$, and $c = 6$.

We next studied the effect of the biological parameters on the cell and tissue emergent dynamics (Figure 2B-E). For each parameter set, ten simulations were performed—although the growth morphogen and cellular forces are deterministic, the cell division plane during mitosis is stochastic. All simulations resulted in a steady-state circular tissue shape, with the number of cells at steady state being modulated by the different biological parameters. The morphogen production constant linearly correlated with the number of cells (Figure 2B), whereas the morphogen degradation rate (Figure 2D) and regulation threshold (Figure 2E) were inversely correlated. Interestingly, the morphogen production constant and the regulation threshold had exactly opposite effects, since they both modulated the same regulatory dynamics (as modeled by a Hill function; see Equation 10). Although the morphogen diffusion constant was positively correlated with the number of cells (Figure 2C), its effect was much lower. In addition to the number of cells at steady state, the morphogen degradation rate also affected the speed at which the steady state was reached (Figure 2D), as a slower degradation rate results in slower equilibrium dynamics. All morphogen production and receptor parameters tested within a two-fold range resulted in a noticeable change in the number of cells at steady state. However, the morphogen diffusion coefficient only had a noticeable effect on the number of cells when changed by a 10-fold difference (Figure 2C). Furthermore, as the diffusion coefficient modulates the morphogen diffusion length, a higher diffusion coefficient results in a larger diffusion area where cells grow and divide, resulting in an increased number of cells and tissue size at steady state (Figure 2C, inset). Crucially, there exists a critical value of the diffusion coefficient above which tissue growth dynamics remain unchanged, as the negative feedback between the growth morphogen concentration and tissue size balances.

In addition to morphogen parameters, the threshold of cell crowding inhibition modulates the dynamics of shape formation. Figure 3 shows the simulations of tissue growth with a single-source morphogen at different cell crowding inhibition thresholds. At a low inhibition threshold, growth

is reduced at low local cell densities, which results in differential tissue expansion at the border towards the direction of low cell density, and hence an irregular tissue shape (Figure 3A). In contrast, at high cell crowding thresholds, growth inhibition occurs only at high cell densities, resulting in more homogeneous growth across the tissue and a faster convergence to a steady-state circular shape (Figure 3B). In addition to affecting shape dynamics, higher cell crowding thresholds resulted in a larger number of cells at steady state because cell growth was inhibited at higher densities (Figure 3C). Overall, the cell crowding threshold plays a significant role in modulating tissue growth dynamics in terms of shape, size, and convergence speed (see Supplementary Video 2).

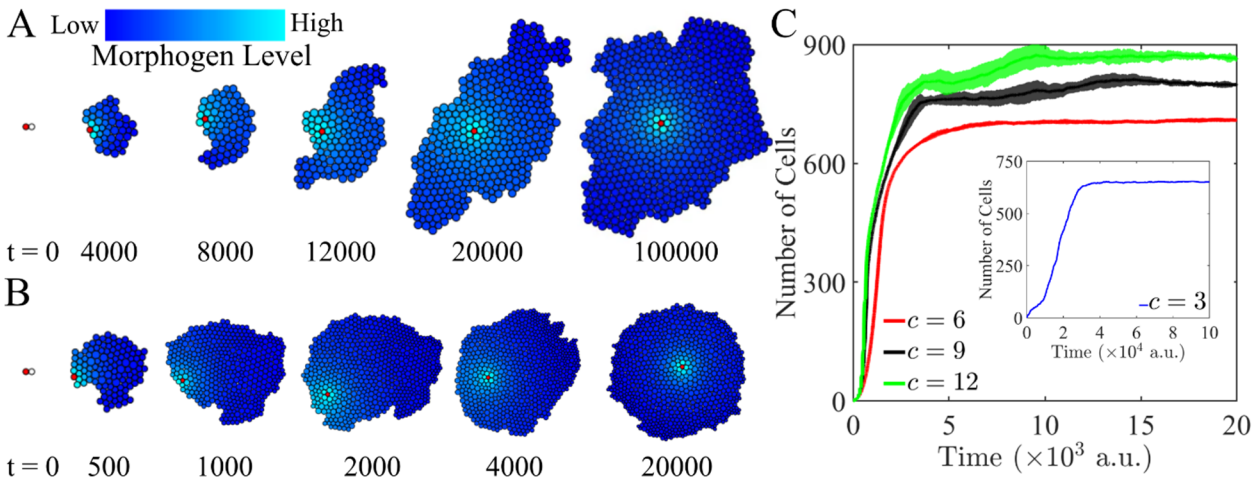

Figure 3. The shape dynamics regulated by a single-source cell depend on the cell-crowding inhibition threshold. A. A low cell crowding inhibition threshold ($c = 3$) inhibits growth at low local cell density, resulting in nonuniform cell proliferation that leads to irregular shapes. **B.** A high cell crowding inhibition threshold ($c = 12$) inhibits growth only at high local cell density, resulting in a circular shape. **C.** The growth curves show how higher cell crowding inhibition thresholds result in a higher number of cells at steady state that are reached at shorter times. The inset shows the growth curve for a low cell crowding inhibition threshold ($c = 3$), which requires a longer time to reach a steady state. All parameter sets were simulated ten times. The plots show average (line) and standard deviation (shaded area). Remaining parameters: $q = 0.1$, $\alpha = 10$, $\lambda = 0.001$, $k = 0.1$.

3.3. Regulation of shape and size by multiple morphogen-source cells

Next, we sought to determine how the number of morphogen-source cells affects the steady-state shape of the tissue. Similar to the previous section, a single diffusible morphogen controls cell

growth; however, more than one non-dividing source cell can express it. Figure 4 shows the simulations of tissue growth with two, three, or four morphogen-source cells (red). Because the growth morphogen concentration is higher near the source cells, higher proliferation rates occur in the cells surrounding the source cells. This higher proliferation, in turn, results in the separation of the source cells from each other until the growth morphogen diffuses to concentrations below its decay, which inhibits cell proliferation and promotes apoptosis. As the source cells acquire a stable distance from each other as the net cell proliferation and apoptosis balance, the resultant steady-state tissue shapes are not circular but can adopt elliptical, triangular, or star shapes depending on the concentration pattern of the growth morphogen modulated by the number of source cells (see also Supplementary Video 3).

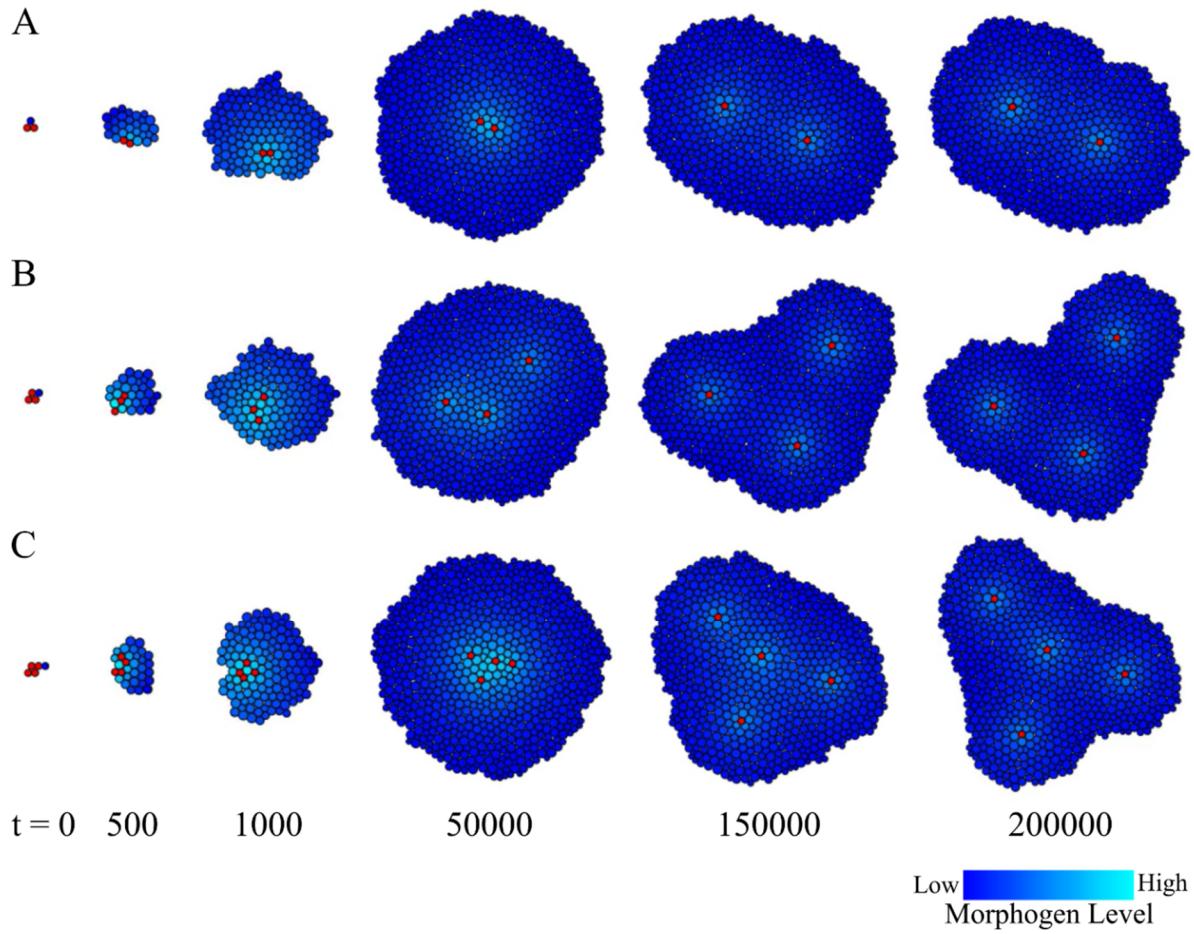

Figure 4. Multiple source cells secreting the same growth morphogen resulted in different steady-state tissue shapes. Cell proliferation induced by the secretion of the growth morphogen results in the source cells (red) moving away from each other. This repulsive effect modulates the concentration levels

of the growth morphogen, resulting in oval (A), triangular (B), or star (C) steady-state tissue shapes under two, three, or four source-morphogen cells, respectively. To maintain the number of cells at steady state equal, the morphogen production constant was scaled accordingly: $q = 0.05$, 0.033, or 0.025 for two, three, or four source cells, respectively. Remaining parameters: $\alpha = 10$, $\lambda = 0.001$, $k = 0.1$, $c = 6$.

3.4. Turing spots and stripes patterns in a growing tissue

Morphogenesis and tissue patterning are not independent processes; rather, they act together through feedback loops to regulate gene expression, size, and shape in growing and differentiating tissues. Next, we studied the feedback process of gene regulation and tissue pattern, size, and shape using the proposed framework. First, we tested the capacity of the model to form spatial patterns of morphogen expression with a regulatory network based on a Turing mechanism, which is known to regulate many biological patterns and shapes (46–48). As before, a diffusing growth morphogen with concentrations m_{i1} modulates cell growth dynamics and is expressed by a single source cell. Additionally, all cells express two other morphogens with concentrations m_{i2} and m_{i3}, respectively, that interact and diffuse across neighboring cells based on Schnakenberg kinetics (49). Continuous reaction-diffusion systems modeled with Schnakenberg kinetics can produce spot or stripe patterns over a relatively large Turing parameter space compared to other Turing models. In this system, the first morphogen self-promotes its expression while inhibiting the expression of the second morphogen. Conversely, the second morphogen inhibits its own expression and promotes the expression of the first morphogen. In this way the production terms of the Turing morphogens are defined as

$$\begin{aligned} Q_{i2} &= q_2 + \gamma\, m_{i2}^2 m_{i3}, \\ Q_{i3} &= q_3 - \gamma\, m_{i2}^2 m_{i3}, \end{aligned} \tag{13}$$

where q_2 and q_3 are the basal expression levels of each morphogen, and γ is a coupling constant. In addition, we introduce a scaling parameter Λ in the Turing morphogens' reaction term that can control the spatial scale of the periodic pattern, such as

$$R_{ik} = \Lambda(Q_{ik} - \lambda_k m_{ik} - g_i m_{ik}). \tag{14}$$

Figure 5 shows the simulations of the spatial patterning dynamics through time in a proliferating and growing tissue domain from a single source cell for the growth morphogen (see Supplementary

Video 4). As before, the growth morphogen from the single source cell modulates tissue growth dynamics, resulting in a stable circular shape. As all the cells implement the reaction-diffusion Turing mechanism, the proliferative tissue dynamically forms a spot pattern that, concomitant with the tissue shape, reaches a stable steady state. The wavelength of the system, that is, the distance between the spot centers, is modulated by the scaling parameter Λ, which also influences the spot size. A small scaling factor $\Lambda = 0.1$ results in a higher wavelength, leading to a single stable spot at the center of the tissue domain (Figure 5A). As the scaling factor Λ is increased to 0.5, the wavelength and spot size decrease, resulting in three stable spots in the same tissue domain (Figure 5B). A further increase in the scaling factor Λ to 2.0 results in a higher number of smaller spots (Figure 5C).

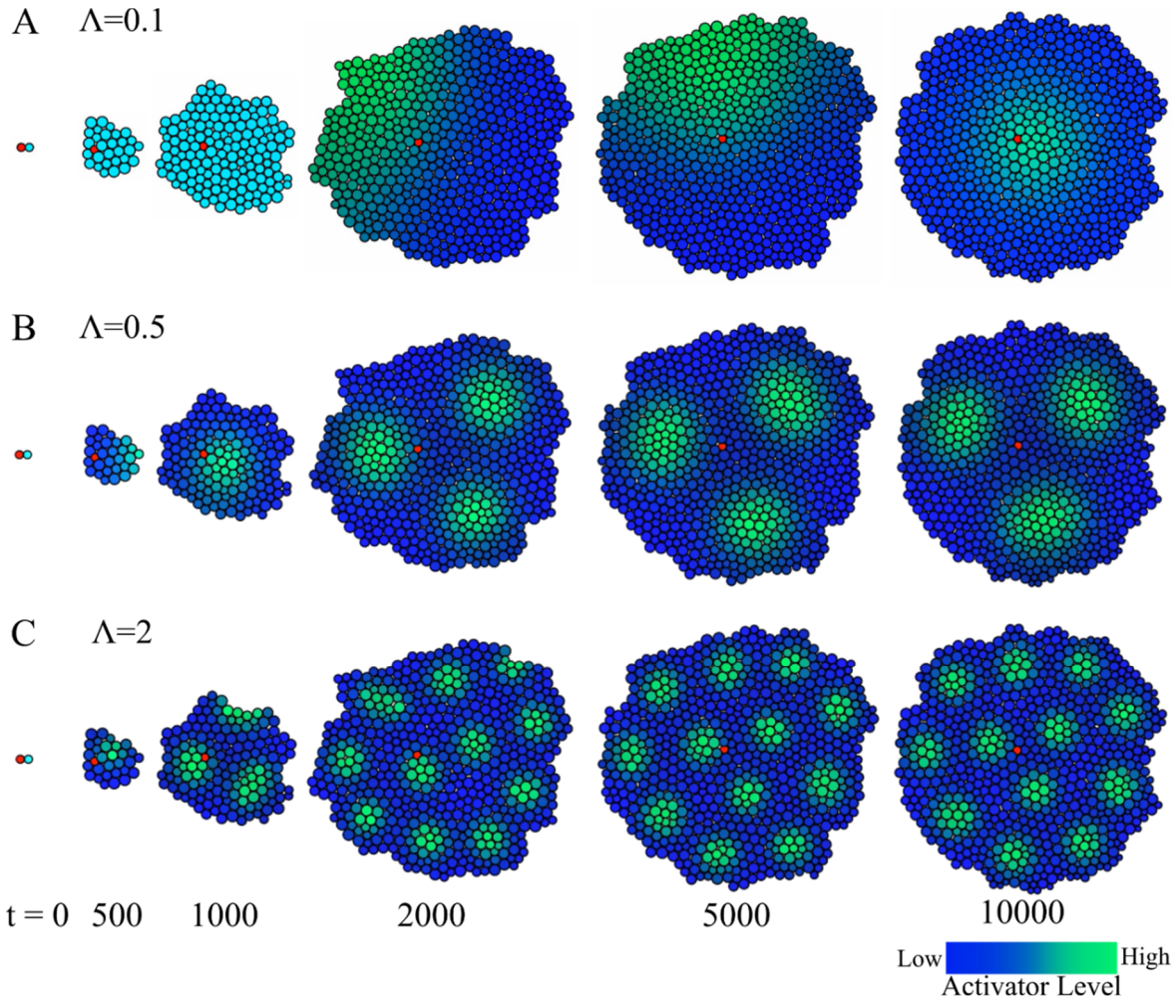

Figure 5. A growing tissue with a single growth morphogen source can produce stable Turing spot patterns at different wavelengths. A single source cell (red) secretes a diffusive growth morphogen,

resulting in a stable circular tissue shape. In addition, all cells include a genetic circuit implementing an activator-inhibitor Schnakenberg Turing mechanism that reacts and diffuses across the domain. The system can produce spot patterns across the growing tissue, reaching a stable, steady-state spatial configuration. **(A-C)** The scaling factor Λ modulates the number and size of the spots. Blue-green indicates the concentration of the activator. Parameters: $q_1 = 0.1, q_2 = 0.1, q_3 = 0.9, \alpha_1 = 10, \alpha_2 = 2,\ \alpha_3 = 40, \lambda_1 = 0.001, \lambda_2 = 1.0, \lambda_3 = 0.1, \gamma = 1.0$.

In addition to spot patterns, a Turing mechanism can produce stripes in a continuous domain. To test the ability of the proposed model to produce stable stripe patterns in a growing tissue, the production term of the inhibitor morphogen was modified such that it is modulated by the activator morphogen, resulting in

$$\begin{aligned} Q_{i2} &= q_2 - (q_3 + 1)m_{i2} + \gamma\, m_{i2}^2 m_{i3}, \\ Q_{i3} &= q_3 m_{i2} - \gamma\, m_{i2}^2 m_{i3}. \end{aligned} \tag{15}$$

Figure 6 shows the simulations through time of the modified Schnakenberg system in a proliferating and growing tissue domain from a single source cell for the growth morphogen (see Supplementary Video 5). As with the spot pattern, the growth morphogen signaling resulted in a stable circular shape, whereas the reaction-diffusion mechanism dynamically produced a stable stripe pattern. Similarly, the scaling parameter Λ modulates the wavelength of the system—in this case, the distance between the stripes. Hence, at the steady-state, increasing values of the scaling parameter Λ results in one, three, or multiple stripes (Figure 6A-C, respectively). Notably, the spot and stripe patterns do not form at high scaling parameter values (data not shown) because the system wavelength becomes smaller than the size of a single cell. Conversely, low values of the scaling parameter may require domain sizes larger than the tissue size; otherwise, the spot and stripe patterns do not form. These analyses demonstrate the versatility of the model for studying periodic pattern formation in dynamic tissue shapes.

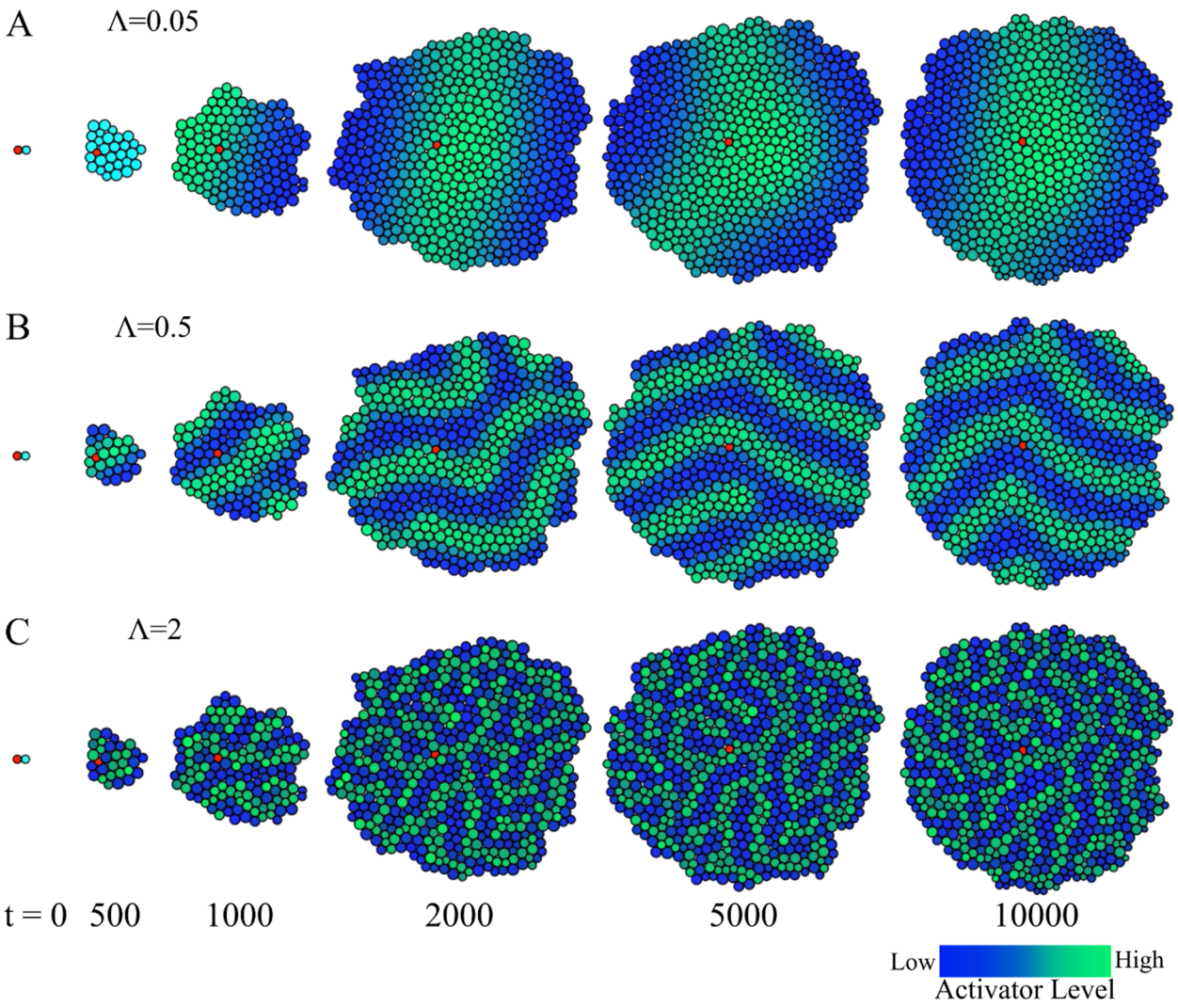

Figure 6. Stable Turing stripe patterns at different wavelengths can also be formed in growing tissues with a single growth morphogen source. When the production term of the inhibitor is also modulated by the activator in the Schnakenberg Turing mechanism, the growing tissue with a single source cell (red) can produce stable stripe patterns instead of spot patterns (see Figure 5). **(A-C)** The scaling factor Λ modulates the number and size of the stripes. Blue-green indicates activator concentration. Parameters: $q_1 = 0.1, q_2 = 3, q_3 = 9, \alpha_1 = 10, \alpha_2 = 3,\ \alpha_3 = 10, \lambda_1 = 0.001, \lambda_2 = 0, \lambda_3 = 0, \gamma = 1.0$.

3.5. Tissue shape controlled by Turing mechanisms

The coupling of gene expression patterning and growth to regulate the shape of a tissue or the whole body is a complex process that is not well understood. Genes such as sonic hedgehog (*Shh*) can act as both morphogens and mitogens to regulate vertebrate development, including patterning, proliferation, growth, and differentiation (20). Modeling the complex interplay between pattern formation, cell proliferation, and tissue growth can provide mechanistic insights into these feedback regulatory processes (22, 34). To investigate the emergence of shapes through shape-morphogen feedback mechanisms, we adapted the proposed Turing system to produce spatial patterns that act as morphogens controlling cell growth. In this way, there are no source cells expressing the growth morphogen; instead, all cells implement the activator-inhibitor system (Equation 13), whereas the activator acts as the growth morphogen and directly regulates cellular growth (Equation 10).

Figure 7 shows different simulations of the Turing system regulating cellular growth dynamics, all resulting in different stable tissue shapes depending on the duration of the developmental period (see also Supplementary Video 6). The initial state included a single cell with equal activator-inhibitor system concentrations. A low growth morphogen threshold $k = 0.1$ (Equation 10) induces cell growth and proliferation during development. As the tissue grows, the Turing system produces different spot patterns that, in turn, regulate cellular proliferation in a feedback loop. After the developmental period, the growth morphogen threshold is increased to $k = 0.4$, which reduces cell proliferation and leads to a steady-state Turing pattern and tissue shape. Figure 7A shows how a short developmental period results in a circular shape with a single Turing morphogen spot that regulates cell proliferation. The high concentration of this growth morphogen at the tissue center (green cells) results in a higher cell proliferation rate that balances with the higher apoptosis rate at the border (blue cells) due to the lower growth morphogen concentration. The proliferation at the center balances with the apoptosis at the border and results in a dynamically stable steady state forming a circular tissue shape. Hence, the circular stable spatial tissue configuration is driven by the feedback loop between the Turing pattern controlling cell proliferation and the resulting tissue shape, where the Turing pattern reacts and diffuses.

Crucially, the length of the developmental period modulates the number of spots, and hence the resulting shape at the steady state (Figure 7 B-F). Longer developmental periods increase apoptosis

and, hence, the number of cells. Because the wavelength of the Turing system is constant, a larger number of spots develop in larger tissues, which in turn can produce different shapes. Figure 7 shows simulations with increased developmental periods that lead to stable steady-state tissue patterns and shapes with one to seven spots. The shapes resulting from the different number of spots included circular, hourglass, triangular, and up to hexagonal for one, two, three, and seven spots, respectively.

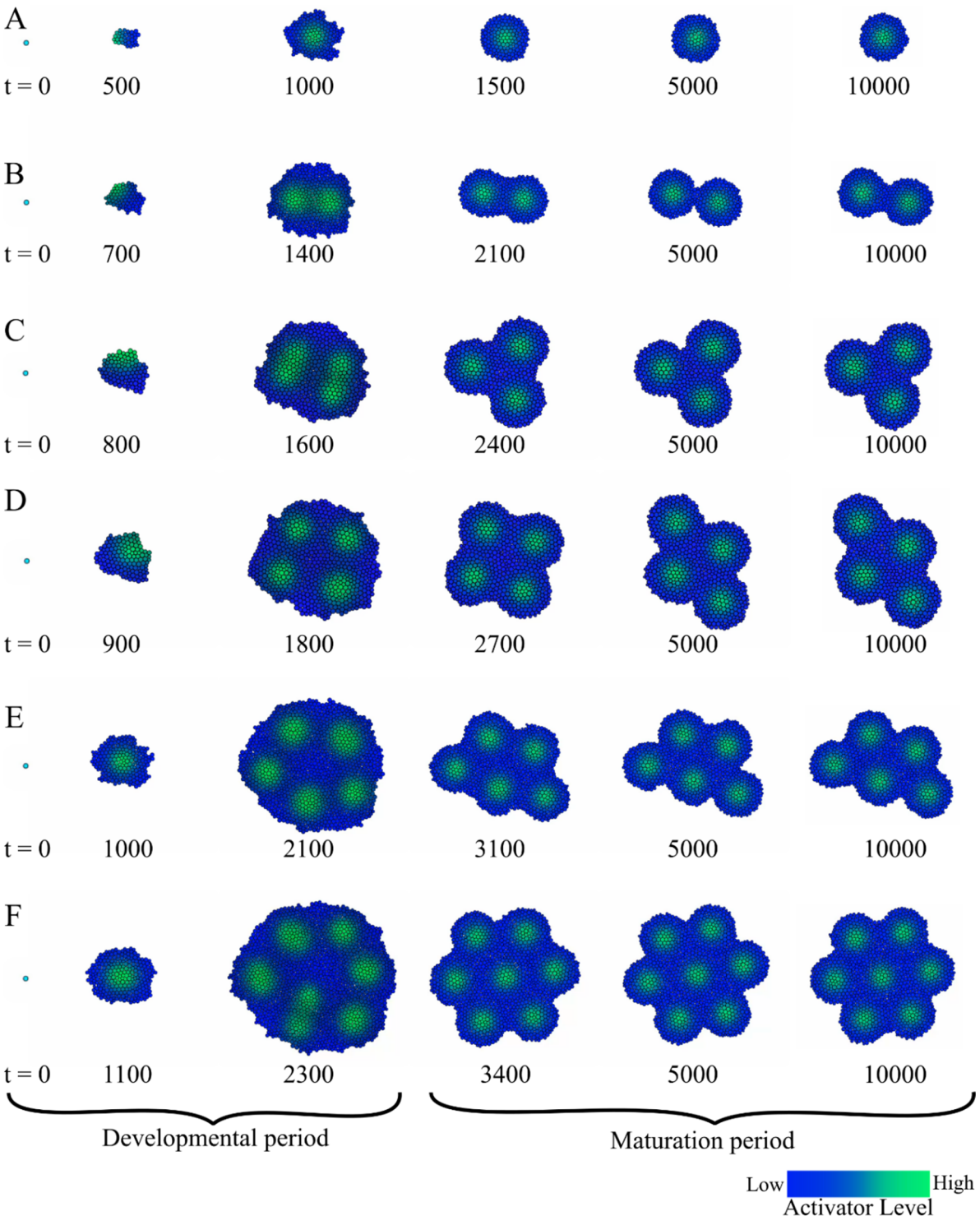

Figure 7. The feedback between a Turing spot mechanism controlling cell proliferation and the resulting tissue growth can produce different stable shapes depending on the length of the developmental period. (A-F) Simulation snapshots of tissue growth governed by the Schnakenberg activator-inhibitor kinetics. The Turing system drives both the spot spatial pattern and the resulting tissue

shape, as the activator morphogen regulates cell growth. A first period of development with high cell proliferation (growth morphogen threshold $k = 0.1$) causes an initial tissue growth, after which a stable dynamic shape is established owing to a lower cell proliferation ($k = 0.4$) The length of the developmental period dictates the number of spots developed and hence the final tissue shape. Parameters: $q_2 = 0.1, q_3 = 0.9, \alpha_2 = 2,\ \alpha_3 = 40, \lambda_2 = 1.0, \lambda_3 = 0.1, \gamma = 1.0$.

In addition to spot patterns, the Schnakenberg system can produce stripe patterns (Figure 6), which can act as morphogen signals for cell proliferation. Figure 8 shows simulations of the stripe-producing Schnakenberg system where the activator regulates cell growth (see also Supplementary Video 7). As before, the initial state included a single cell with equal morphogen concentrations. The simulation was divided into a developmental period with a low morphogen threshold ($k = 0.5$) resulting in high cell proliferation, followed by a stable period with a high morphogen threshold ($k = 2.5$) causing a balance between cell proliferation and apoptosis. Although the number of cells reached a steady state, the stripe pattern, in contrast to the spot pattern, did not result in a stable tissue shape. Because the activator stripes reach the edge of the tissue, cell proliferation is high in these locations, leading to shape instability and dynamic continuous reconfiguration of the stripe pattern. The overall size of the tissue is controlled by the length of the developmental period; yet, the resulting dynamic tissue shapes are similar.

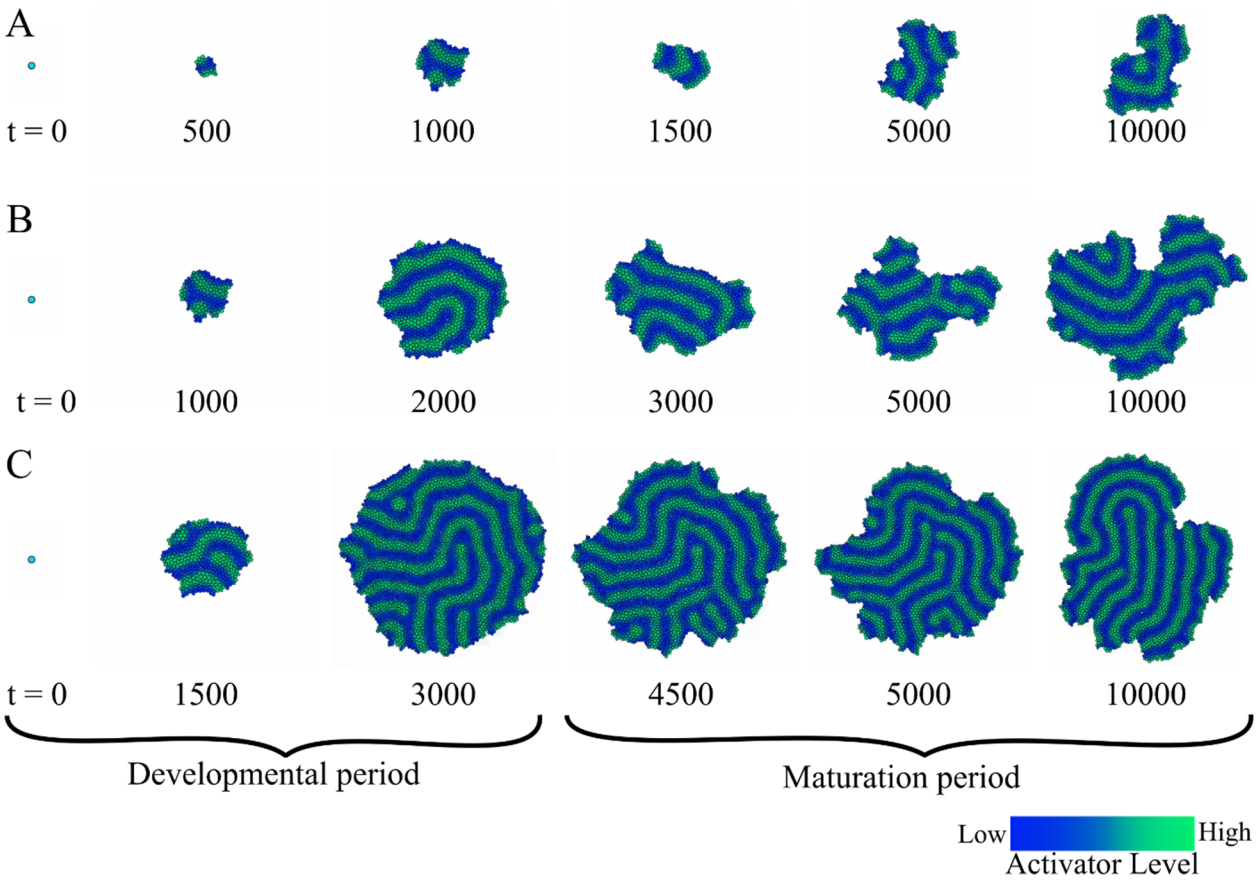

Figure 8. A Schnakenberg stripe mechanism controlling cell proliferation results in dynamic tissue shapes. (A-C) Simulation snapshots of tissue growth governed by Schnakenberg activator-inhibitor kinetics driving the stripe spatial pattern and resulting tissue shape. During the development period (growth morphogen threshold $k = 0.5$) the tissue grows, which is followed by a stable period ($k = 0.4$) when cell proliferation and apoptosis are balanced. An increased developmental period results in larger tissue sizes; however, the tissue shape dynamically changes due to stripe-driven cell proliferation at the tissue border. Parameters: $q_2 = 3, q_3 = 9, \alpha_2 = 3,\ \alpha_3 = 10, \lambda_2 = 0, \lambda_3 = 0, \gamma = 1.0$.

Although the stripe-forming Schnakenberg mechanism, which controls cell proliferation, produces globular tissue shapes (Figure 8), a stripe Turing system has the potential to produce a single elongated shape. For this, a single stripe with a high activator concentration at the midline and low concentration at the border could form a stable elongated shape. Hence, the high proliferation rate at the midline could balance the apoptosis at the border to form a stable filament shape. At the extreme of the stripes, a high concentration of the activator could induce stripe growth. We tested this hypothesis with a molecularly plausible Gierer-Meinhardt model of reaction-diffusion mechanisms (50–52) defined as

$$Q_{i2} = q_2 + \gamma \frac{m_{i1}^2}{m_{i2}(1 + \delta m_{i1}^2)}, \qquad (16)$$
$$Q_{i3} = q_2 + \gamma\, m_{i1}^2.$$

where q_1 and q_2 are the basal expression levels of each morphogen, γ is a coupling constant, and δ is the inverse of the production threshold for the activator. As before, a scaling parameter Λ controls the spatial scale of the periodic pattern (Equation 14).

Figure 9 shows the simulations of the Gierer-Meinhardt model where the activator morphogen regulates cell growth (see also Supplementary Video 8). Starting with a single cell, the tissue proliferates isometrically until a stripe pattern forms. The high proliferation rate at the stripe midline is balanced with the high apoptosis rate at the lateral border, resulting in a filament shape (Figure 9B). The activator inducing a high proliferation rate is also high at the tip of the filament, which causes continuous growth of the filament. As the scaling factor Λ decreases to 0.05, both the wavelength and stripe size increase, resulting in wider stripes within the tissue domain (Figure 9A). Conversely, increasing the scaling factor Λ to 0.5 leads to a higher number of thinner stripes, resulting in a more circular shape (Figure 9C).

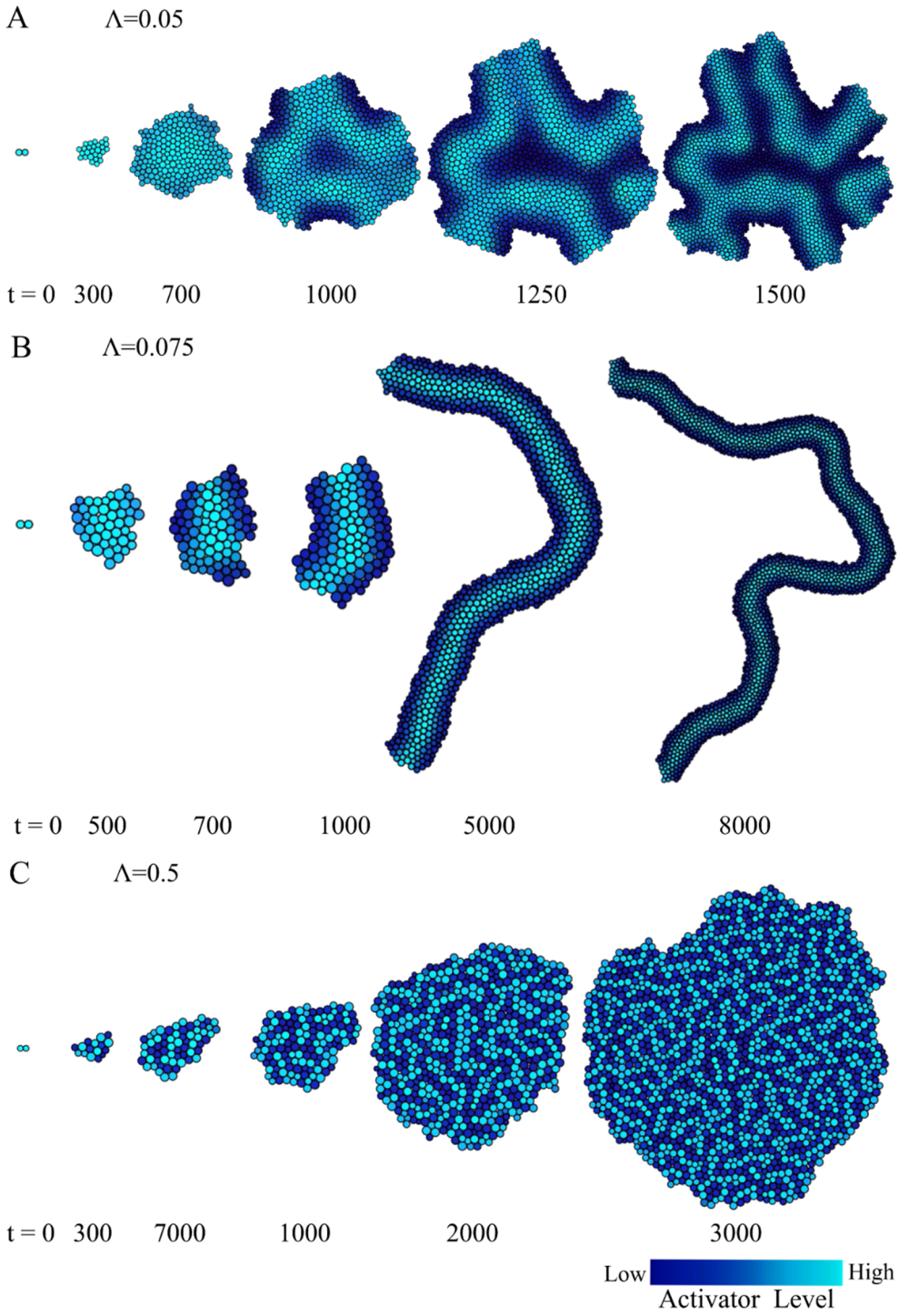

Figure 9. A Gierer-Meinhardt stripe mechanism controlling cell proliferation results in growing filament tissue shapes. Simulation snapshots of tissue growth governed by Gierer-Meinhardt reaction-diffusion kinetics driving the formation of a filament tissue shape formed by a single stripe. **(A-C)** The scaling factor Λ modulates the pattern and shape. Parameters: $q_2 = 0, q_3 = 0, \alpha_2 = 0.1,\ \alpha_3 = 2,\ \lambda_2 = 1.2, \lambda_3 = 1.0, \gamma = 1.0, \delta = 0.4$.

4. Discussion

Here, we proposed a mathematical framework for morphogen-mediated tissue growth dynamics in two-dimensional space, which provides a novel approach to investigate the role of the feedback between mechano-chemical signaling pathways and tissue-level shapes. The model is based on mechano-chemical interactions that govern cellular behaviors to demonstrate how cell-level phenomena, such as growth, proliferation, and apoptosis, influence tissue-scale dynamics. Conversely, the overall tissue shape and size feedback into the regulation of morphogen patterns that can diffuse through the tissue formed by the cells, closing the loop between cellular behaviors and emergent shapes. The model also includes cell death and cell proliferation, which are essential for the formation of steady-state tissue configurations in terms of shape, size, and patterning. Crucially, the model does not require any superimposed lattice; yet, it can explain the formation of tissue patterning with an increase in performance and applicability.

The proposed framework was employed to study tissue morphogenesis driven by specialized cells through the production of a morphogen regulating cell growth. The results show how different tissue shapes emerged depending on the number of source cells. For a single source cell, a stable circular tissue shape was formed at the steady state, whereas a stable elliptical tissue shape resulted from two source cells. As the number of source cells increased, the shape became increasingly complex. A parametric analysis of the single-source cell system revealed that the morphogen diffusion constant, degradation rate, and regulation threshold all play crucial roles in tissue growth dynamics and final shape size. Finally, the results showed that the time to reach steady state and stable tissue size are highly sensitive to the parameters that regulate the intracellular morphogen dynamics and their microenvironment.

The model was then extended to investigate the underlying feedback mechanism between patterning and cellular behaviors and their role in the regulation of morphogenesis. First, we studied how the pattern dynamics of a Turing activator-inhibitor system can evolve concomitantly with tissue growth. The results showed how cell fate specification can emerge from an intracellular activator-inhibitor system as the pattern forms and scales with the overall tissue size. Both spot and stripe patterns can be observed depending on the regulatory interactions between morphogens in the Turing system. Crucially, closing the loop between cell growth dynamics and tissue patterning by regulating cell growth with a Turing morphogen results in self-organized stable

tissue shapes, providing important insights into the coupling between mechanochemical signals and tissue dynamics. These experiments showed how the threshold value of the growth morphogen significantly contributes to a stable morphological state. For example, in the spot pattern dynamics, various stable morphological states were observed depending on the switching time of the threshold value for the growth control morphogen. In contrast, the stripe pattern dynamics resulted in dynamic tissue shapes, including growing filaments, owing to the growing front at the tissue border.

5. Conclusions

The proposed framework linking cellular behaviors, patterning, and tissue shapes provides a robust theoretical basis for studying dynamic tissue morphogenesis and patterning. This work could be applied to understand the mechanisms driving specific biological processes during development and regeneration. Crucially, the proposed lightweight approach does not require a superimposed lattice to compute diffusion, which will facilitate its integration into machine learning algorithms that can infer models for particular patterns and shapes (53, 54). The predictive models can then be validated experimentally at the level of whole-body tissue phenotypes (55, 56) and gene expression patterns using whole-mount in situ hybridization assays (57). Overall, the analysis presented in this study provides evidence of the significant role of the regulatory feedback between morphogens and cell dynamics in controlling target tissue and whole-body shapes during morphogenesis, paving the way for new insights into tissue engineering and regenerative medicine.

Acknowledgements

We thank the members of the Lobo Lab for helpful discussions. This work was supported by the National Institute of General Medical Sciences of the National Institutes of Health under award number R35GM137953. The content is solely the responsibility of the authors and does not necessarily represent the official views of the National Institutes of Health. Computations used the UMBC High Performance Computing Facility (HPCF) supported by the NSF MRI program grants CNS-1920079 and OAC-1726023.

Competing interests

The authors declare no competing interests.

References

1. Farahani, P.E., and C.M. Nelson. 2022. Revealing epithelial morphogenetic mechanisms through live imaging. *Current Opinion in Genetics & Development*. 72:61–68.

2. Collinet, C., and T. Lecuit. 2021. Programmed and self-organized flow of information during morphogenesis. *Nat Rev Mol Cell Biol*. 22:245–265.

3. Picker, A., F. Cavodeassi, A. Machate, S. Bernauer, S. Hans, G. Abe, K. Kawakami, S.W. Wilson, and M. Brand. 2009. Dynamic Coupling of Pattern Formation and Morphogenesis in the Developing Vertebrate Retina. *PLoS Biol*. 7:e1000214.

4. Eldred, M.K., M. Charlton-Perkins, L. Muresan, and W.A. Harris. 2017. Self-organising aggregates of zebrafish retinal cells for investigating mechanisms of neural lamination. *Development*. dev.142760.

5. Salbreux, G., L.K. Barthel, P.A. Raymond, and D.K. Lubensky. 2012. Coupling Mechanical Deformations and Planar Cell Polarity to Create Regular Patterns in the Zebrafish Retina. *PLoS Comput Biol*. 8:e1002618.

6. Aegerter-Wilmsen, T., M.B. Heimlicher, A.C. Smith, P.B. De Reuille, R.S. Smith, C.M. Aegerter, and K. Basler. 2012. Integrating force-sensing and signaling pathways in a model for the regulation of wing imaginal disc size. *Development*. 139:3221–3231.

7. Heisenberg, C.-P., and Y. Bellaïche. 2013. Forces in Tissue Morphogenesis and Patterning. *Cell*. 153:948–962.

8. Lobo, D., W.S. Beane, and M. Levin. 2012. Modeling Planarian Regeneration: A Primer for Reverse-Engineering the Worm. *PLoS Comput Biol*. 8:e1002481.

9. Keller, R. 2012. Physical Biology Returns to Morphogenesis. *Science*. 338:201–203.

10. Hopyan, S., J. Sharpe, and Y. Yang. 2011. Budding behaviors: Growth of the limb as a model of morphogenesis. *Dev. Dyn.* 240:1054–1062.

11. Ko, J.M., R. Mousavi, and D. Lobo. 2022. Computational Systems Biology of Morphogenesis. In: Cortassa S, MA Aon, editors. Computational Systems Biology in Medicine and Biotechnology: Methods and Protocols. New York, NY: Springer US. pp. 343–365.

12. Lu, P., G. Minowada, and G.R. Martin. 2006. Increasing *Fgf4* expression in the mouse limb bud causes polysyndactyly and rescues the skeletal defects that result from loss of *Fgf8* function. *Development*. 133:33–42.

13. Boulet, A.M., A.M. Moon, B.R. Arenkiel, and M.R. Capecchi. 2004. The roles of Fgf4 and Fgf8 in limb bud initiation and outgrowth. *Developmental Biology*. 273:361–372.

14. Steinberg, M.S. 1958. On the Chemical Bonds between Animal Cells. A Mechanism for Type-Specific Association. *The American Naturalist*. 92:65–81.

15. Townes, P.L., and J. Holtfreter. 1955. Directed movements and selective adhesion of embryonic amphibian cells. *J. Exp. Zool.* 128:53–120.

16. Ko, J.M., and D. Lobo. 2019. Continuous Dynamic Modeling of Regulated Cell Adhesion: Sorting, Intercalation, and Involution. *Biophysical Journal*. 117:2166–2179.

17. Hagolani, P.F., R. Zimm, M. Marin-Riera, and I. Salazar-Ciudad. 2019. Cell signaling stabilizes morphogenesis against noise. *Development*. 146:dev179309.

18. Salm, M., and L.M. Pismen. 2012. Chemical and mechanical signaling in epithelial spreading. *Phys. Biol.* 9:026009.

19. Kicheva, A., and J. Briscoe. 2023. Control of Tissue Development by Morphogens. *Annual Review of Cell and Developmental Biology*. 39:null.

20. Groves, I., M. Placzek, and A.G. Fletcher. 2020. Of mitogens and morphogens: modelling Sonic Hedgehog mechanisms in vertebrate development. *Phil. Trans. R. Soc. B*. 375:20190660.

21. Jung, H.-S., P.H. Francis-West, R.B. Widelitz, T.-X. Jiang, S. Ting-Berreth, C. Tickle, L. Wolpert, and C.-M. Chuong. 1998. Local Inhibitory Action of BMPs and Their Relationships with Activators in Feather Formation: Implications for Periodic Patterning. *Developmental Biology*. 196:11–23.

22. Economou, A.D., A. Ohazama, T. Porntaveetus, P.T. Sharpe, S. Kondo, M.A. Basson, A. Gritli-Linde, M.T. Cobourne, and J.B.A. Green. 2012. Periodic stripe formation by a Turing mechanism operating at growth zones in the mammalian palate. *Nat Genet*. 44:348–351.

23. Moustakas-Verho, J.E., R. Zimm, J. Cebra-Thomas, N.K. Lempiäinen, A. Kallonen, K.L. Mitchell, K. Hämäläinen, I. Salazar-Ciudad, J. Jernvall, and S.F. Gilbert. 2014. The origin and loss of periodic patterning in the turtle shell. *Development*. 141:3033–3039.

24. Morishita, Y., and Y. Iwasa. 2008. Growth Based Morphogenesis of Vertebrate Limb Bud. *Bull. Math. Biol.* 70:1957–1978.

25. Mateus, R., J.F. Fuhrmann, and N.A. Dye. 2021. Growth across scales: Dynamic signaling impacts tissue size and shape. *Current Opinion in Cell Biology*. 73:50–57.

26. Sharpe, J. 2017. Computer modeling in developmental biology: growing today, essential tomorrow. *Development*. 144:4214–4225.

27. Cockerell, A., L. Wright, A. Dattani, G. Guo, A. Smith, K. Tsaneva-Atanasova, and D.M. Richards. 2023. Biophysical models of early mammalian embryogenesis. *Stem Cell Reports*. 18:26–46.

28. Glen, C.M., M.L. Kemp, and E.O. Voit. 2019. Agent-based modeling of morphogenetic systems: Advantages and challenges. *PLoS Comput Biol*. 15:e1006577.

29. Van Liedekerke, P., M.M. Palm, N. Jagiella, and D. Drasdo. 2015. Simulating tissue mechanics with agent-based models: concepts, perspectives and some novel results. *Comp. Part. Mech.* 2:401–444.

30. Pleyer, J., and C. Fleck. 2023. Agent-based models in cellular systems. *Front. Phys.* 10.

31. West, J., M. Robertson-Tessi, and A.R.A. Anderson. 2023. Agent-based methods facilitate integrative science in cancer. *Trends in Cell Biology*. 33:300–311.

32. Mathias, S., A. Coulier, A. Bouchnita, and A. Hellander. 2020. Impact of Force Function Formulations on the Numerical Simulation of Centre-Based Models. *Bull Math Biol*. 82:132.

33. Ko, J.M., W. Reginato, A. Wolff, and D. Lobo. 2024. Mechanistic regulation of planarian shape during growth and degrowth. *Development*. 151:dev202353.

34. Krause, A.L., E.A. Gaffney, and B.J. Walker. 2023. Concentration-Dependent Domain Evolution in Reaction–Diffusion Systems. *Bull Math Biol*. 85:14.

35. Ramezani, A., S. Britton, R. Zandi, M. Alber, A. Nematbakhsh, and W. Chen. 2023. A multiscale chemical-mechanical model predicts impact of morphogen spreading on tissue growth. *npj Syst Biol Appl*. 9:1–12.

36. Kaul, H., N. Werschler, R.D. Jones, M.M. Siu, M. Tewary, A. Hagner, J. Ostblom, D. Aguilar-Hidalgo, and P.W. Zandstra. 2023. Virtual cells in a virtual microenvironment recapitulate early development-like patterns in human pluripotent stem cell colonies. *Stem Cell Reports*. 18:377–393.

37. Osborne, J.M., A.G. Fletcher, J.M. Pitt-Francis, P.K. Maini, and D.J. Gavaghan. 2017. Comparing individual-based approaches to modelling the self-organization of multicellular tissues. *PLoS Computational Biology*. 13:e1005387.

38. Okuda, S., T. Miura, Y. Inoue, T. Adachi, and M. Eiraku. 2018. Combining Turing and 3D vertex models reproduces autonomous multicellular morphogenesis with undulation, tubulation, and branching. *Sci Rep*. 8:2386.

39. Delile, J., M. Herrmann, N. Peyriéras, and R. Doursat. 2017. A cell-based computational model of early embryogenesis coupling mechanical behaviour and gene regulation. *Nat Commun*. 8:13929.

40. Purcell, E.M. 1977. Life at low Reynolds number. *American Journal of Physics*. 45:3–11.

41. Vazquez, K., A. Saraswathibhatla, and J. Notbohm. 2022. Effect of substrate stiffness on friction in collective cell migration. *Sci Rep*. 12:2474.

42. Shu, W., and C.N. Kaplan. 2023. A multiscale whole-cell theory for mechanosensitive migration on viscoelastic substrates. *Biophysical Journal*. 122:114–129.

43. Truskey, G.A., F. Yuan, and D.F. Katz. 2009. Transport phenomena in biological systems. 2nd ed. Upper Saddle River, N.J: Pearson Prentice Hall.

44. Law, T.R., J. Hancox, S.A. Wright, and S.A. Jarvis. 2019. An algorithm for computing short-range forces in molecular dynamics simulations with non-uniform particle densities. *Journal of Parallel and Distributed Computing*. 130:1–11.

45. Bortner, C.D., and J.A. Cidlowski. 2002. Apoptotic volume decrease and the incredible shrinking cell. *Cell Death & Differentiation*. 9:1307–1310.

46. Maini, P.K., T.E. Woolley, R.E. Baker, E.A. Gaffney, and S.S. Lee. 2012. Turing's model for biological pattern formation and the robustness problem. *Interface Focus.* 2:487–496.

47. Okuda, S., T. Miura, Y. Inoue, T. Adachi, and M. Eiraku. 2018. Combining Turing and 3D vertex models reproduces autonomous multicellular morphogenesis with undulation, tubulation, and branching. *Sci Rep*. 8:2386.

48. Herath, S., and D. Lobo. 2020. Cross-inhibition of Turing patterns explains the self-organized regulatory mechanism of planarian fission. *Journal of Theoretical Biology*. 485:110042.

49. Schnakenberg, J. 1979. Simple chemical reaction systems with limit cycle behaviour. *Journal of Theoretical Biology*. 81:389–400.

50. Gierer, A., and H. Meinhardt. 1972. A theory of biological pattern formation. *Kybernetik*. 12:30–39.

51. Koch, A.J., and H. Meinhardt. 1994. Biological pattern formation: from basic mechanisms to complex structures. *Rev. Mod. Phys.* 66:1481–1507.

52. Yamaguchi, M., E. Yoshimoto, and S. Kondo. 2007. Pattern regulation in the stripe of zebrafish suggests an underlying dynamic and autonomous mechanism. *Proc. Natl. Acad. Sci. U.S.A.* 104:4790–4793.

53. Mousavi, R., and D. Lobo. 2024. Automatic design of gene regulatory mechanisms for spatial pattern formation. *npj Syst Biol Appl*. 10:1–13.

54. Mousavi, R., S.H. Konuru, and D. Lobo. 2021. Inference of dynamic spatial GRN models with multi-GPU evolutionary computation. *Briefings in Bioinformatics*. 22:1–11.

55. Lobo, D. 2022. Formalizing Phenotypes of Regeneration. In: Blanchoud S, B Galliot, editors. Whole-Body Regeneration: Methods and Protocols. New York, NY: Springer US. pp. 663–679.

56. Roy, J., E. Cheung, J. Bhatti, A. Muneem, and D. Lobo. 2020. Curation and annotation of planarian gene expression patterns with segmented reference morphologies. *Bioinformatics*. 36:2881–2887.

57. Wolff, A., C. Wagner, J. Wolf, and D. Lobo. 2022. In situ probe and inhibitory RNA synthesis using streamlined gene cloning with Gibson assembly. *STAR Protocols*. 3:101458.